Thermogelling Properties of Triblock Copolymers in the Presence of Hydrophilic Fe3O4 Nanoparticles and Surfactants

ARTICLE *in* LANGMUIR · JULY 2012

Impact Factor: 4.46 · DOI: 10.1021/la302310y · Source: PubMed

2 AUTHORS, INCLUDING:

John Philip
Indira Gandhi Centre for Atomic Research
179 PUBLICATIONS **3,149** CITATIONS

Langmuir

Article

pubs.acs.org/Langmuir

Thermogelling Properties of Triblock Copolymers in the Presence of Hydrophilic Fe_3O_4 Nanoparticles and Surfactants

J. S. Nambam and John Philip*

SMARTS, Metallurgy and Materials Group, Indira Gandhi Centre for Atomic Research, Kalpakkam 603102, Tamil Nadu, India

ABSTRACT: We investigate the supramolecular structure formed by thermogelation of a triblock polymer in the presence of nanoparticles and surfactant using rheometry and small-angle X-ray scattering (SAXS). The triblock copolymer, nanoparticle, and surfactant used in this study are poly(oxyethylene−oxypropylene−oxyethylene), Pluronic F108, Fe_3O_4 nanoparticles, and sodium dodecyl surfactant, respectively. Addition of 1−5 wt % of Fe_3O_4 nanoparticle, of average particle size ∼10 nm, in a weak template of F108 (15 wt %) shows a decrease in the onset of gelation temperature and dramatic alteration in the viscoelastic moduli. The nanocomposite samples show a linear viscoelastic regime up to 5% strain. The SAXS measurement shows that the intermicellar spacing of the supramolecular structure of pure F108 is ∼16.5 nm, and the supramolecular structure is destroyed when nanoparticles and surfactants are incorporated in it. Further, the addition of anionic surfactant to nanocomposites leads to a dramatic reduction in the viscoelastic properties due to strong electrostatic barrier imparted by the surfactant headgroup that prevents the formation of hexagonally ordered micelles. Our results show that the thermogelation is due to the clustering of nanoparticles into a fractal network rather than a close-packed F108 micelles, in agreement with the recent findings in Pluronic F127−laponite systems.

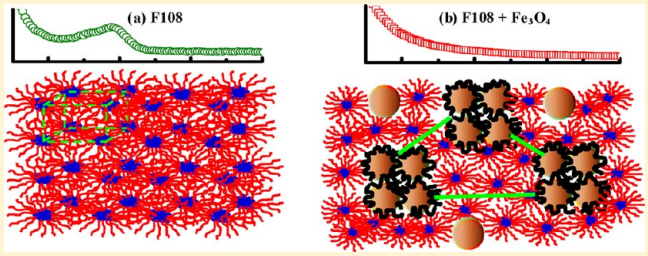

1. INTRODUCTION

Amphiphilic triblock copolymers PEO_m−PPO_n−PEO_m, (where PEO stands for poly(ethylene oxide) and PPO stands for poly(propylene oxide)), commonly known as Pluronics, form self-assembled structures in selective solvents.[1] The self-aggregation arises from the limited and temperature-dependent solubility of the PPO block, which gives rise to aggregates with a hydrophobic, water-free core surrounded by more hydrophilic and hydrated PEO blocks.[2,3] Long-range order in these systems occurs when the number of micellar aggregates (spherical, cylindrical, or planar) exceeds the crystallization volume fraction. The repulsion between the monodisperse spherical micelles drives the formation of cubic phase (face-centered cubic or body-centered cubic) that persists over macroscopic length scale.[4−8] The temperature-induced micellation and the transformation of a low-viscosity liquid to an elastic solid, upon heating above a critical temperature, popularly known as thermogelling,[9] have potential applications in drug delivery[10] and tissue engineering, paints, microfluidic devices, fire fighting, etc. As a result, there have been a focus on synthesis of functional water-soluble copolymers with controlled structures[11] and systematic studies on interactions of nanoparticle dispersions under various conditions.[12−14]

Various characterization techniques such as rheology, small-angle neutron scattering (SANS),[15] X-ray diffraction (XRD), and light scattering have been used to investigate the supramolecular structure of triblock copolymers.[7,10,14−43] Very recently, the polymer−nanoparticle composite materials have been a topic of interest among researchers due to their synergistic hybrid properties.[9,12,44−60] Such composite nanoscale structures made of soft polymeric materials and hard metallic materials can form hybrid nanomaterials with interesting optical, magnetic, electronic, and catalytic properties.[13,61]

Starr et al.[62] have investigated the mechanism of controlling clustering of nanoparticles in polymer−nanocomposites. It has been shown that the introduction of magnetic particles in polyacrylamide gels can enhance their Young modulus.[63] Studies on the influence of added disklike synthetic clay particles (Laponite RDS) on rheology and structure of Pluronic P123 show that the Laponite particles drives a transition from a hexagonal phase of rodlike micelles at low temperature to a lamellar phase at high temperature.[56] The shear alignment of binary crystals of polymeric micelles and small particles, demonstrated using SANS,[50] show that the binary crystals align at significantly lower shear rates compared to neat micellar crystals. The effect of laponite clay particles on thermal and rheological properties of Pluronics triblock copolymer was also investigated.[45,47] The thermogelling studies in aqueous fluids containing low concentrations of Pluronics F127 and laponite nanoparticles show that the thermogelling occur due to depletion flocculation of laponite particles into a network by spherical micelles.[9] There are also a few systematic studies on triblock copolymer−Fe_3O_4 nanocomposites.[44,64,65] Thermoreversible gelation studies of aqueous ferrofluids in triblock copolymer P123 show a reversible temperature-triggered

Received: June 7, 2012
Revised: July 27, 2012
Published: July 30, 2012

   dx.doi.org/10.1021/la302310y | *Langmuir* 2012, 28, 12044−12053

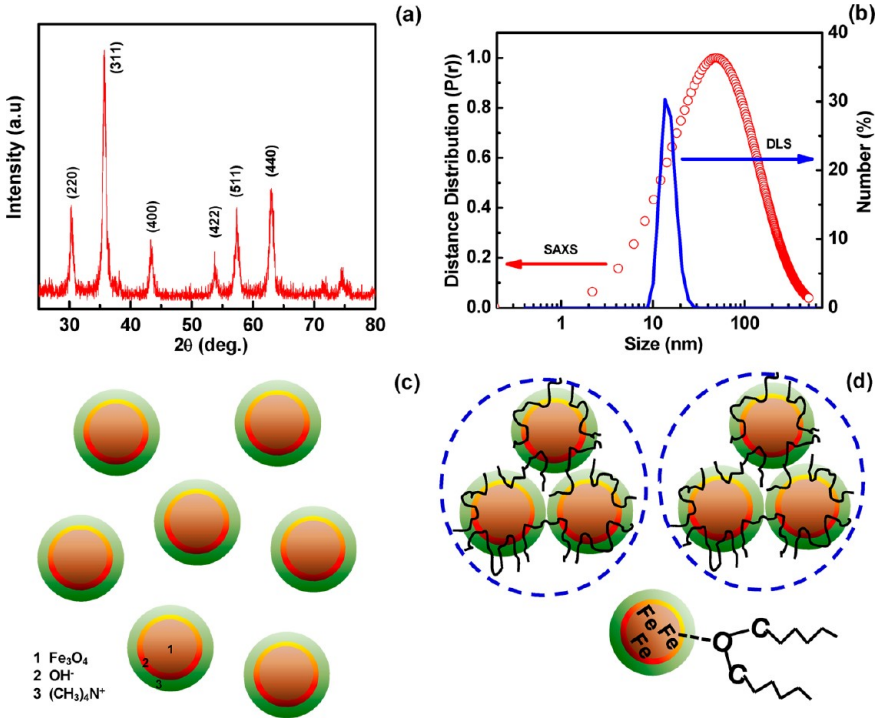

Figure 1. (a) XRD pattern of the Fe_3O_4 nanoparticles. (b) Size distribution profile of 25 wt % F108 with 5% Fe_3O_4 obtained from SAXS (red circle) and the size distribution of primary particle obtained from DLS (blue). (c) Schematic of TMAOH-coated Fe_3O_4 where the nanoparticles have diffuse layer of negative hydroxide ions. (d) Schematic of binding of F108 molecules on nanoparticles and agglomeration of surfactant capped magnetic nanoparticles.

transition from a cubic hard gel to a hexagonal gel.[44,66] Pluronic F127-based magneto-responsive hydrogels are produced using magnetite nanoparticles of low concentrations (<2 wt %).[67] The recent studies on nanocomposite hydrogels reveal that they exhibit better mechanical properties under external magnetic or electric fields.[68−70] Such stimuli-driven composite gels can have potential applications in actuators,[71] microfluidic devices,[72] drug delivery, and hyperthermia.[67,73,74] For development of templates for various applications such as drug delivery and tissue engineering, an understanding of stoichiometry of particles and template sites is a prerequisite. Although nanocomposites of pluronic are studied, there are no studies on the effect of added surfactants on their physical properties. As nanoparticles in dispersions are often stabilized with surfactants, the effect of surfactant on mechanical properties of nanocomposites is very important from application point of view. This study is aimed at providing insight into the microstructural evolution of nanocomposites in presence of surfactants. Here, we try to address the following questions: How does the supramolecular structure of triblock copolymer behave in the presence of nanoparticles and surfactants? Where do the particles sit in the micellar templates, when the particles size is larger than the micelle size? How the presence of nanoparticles and surfactants affect the mechanical and gelation properties of nanocomposites? We use dynamic rheology and SAXS to probe the above aspects.

2. MATERIALS AND METHODS

Poly(ethylene oxide)−poly(propylene oxide)−poly(ethylene oxide) triblock copolymer F108 was purchased from Sigma. The chemical composition of this pluronic is PEO_{141}−PPO_{44}−PEO_{141} with a nominal molar mass of 14 600 g mol^{-1}. All chemicals were used without further purification. Stock solution of the copolymer was prepared using Milli-Q water with resistivity value of 18.2 mΩ·cm. The samples are equilibrated for 48 h before measurements.

The synthesis of magnetite nanoparticles is carried out by precipitating iron salts in alkaline medium. Ferrous sulfate heptahydrate ($FeSO_4·7H_2O$), ferric chloride hexahydrate ($FeCl_3·6H_2O$), 25% aqueous ammonia, oleic acid, 35% hydrochloric acid (HCl), hexane, and acetone procured from E-Merck are used for the synthesis. All the chemicals used are GR grade and used without any further purification. The iron salts used are freshly prepared 0.2 M $FeSO_4·7H_2O$ and 0.4 M $FeCl_3·6H_2O$.[75] To prepare stable water-based magnetite nanofluid, particles are stabilized with tetramethylammonium hydroxide surfactant ($C_4H_{13}NO$). The magnetite nanoparticles prepared by this method are washed with triply distilled water for several times until the pH become 7 to remove the ionic impurities trapped or adhered to the particles. The solution is tested for Cl^- ions with silver nitrate solution. After repeated washings, the particles are coated with tetramethylammonium hydroxide (TMAOH). The surface active species offer electrostatic stabilization for magnetite nanoparticles, thus preventing the formation of agglomerates. The liquidlike behavior of Pluronics F108 at lower temperatures enables preparation of stable and homogeneous dispersion of hydrophilic iron oxide nanoparticles. With increasing temperature of nanoparticles−polymer solution, micellar crystal are formed due to the excluded volume interactions that drive the 3D organization of the hydrophilic nanoparticles.[24,53]

After preparing polymer−nanoparticle composites, the samples were left to equilibrate for 1 week before measurements. The rheological behavior of dispersions is studied with a rotational rheometer (Anton Paar Physica MCR 301) with cone and plate geometry. Dynamic frequency experiments were performed in the linear viscoelastic regime, as measured by dynamic strain-sweep experiments. The temperature of the sample is maintained using a Peltier-based temperature controller, and the experiments are performed after equilibrating the sample temperature for about 30 min.

The samples were characterized for phase identity by X-ray diffraction using Rigaku Ultima IV X-ray diffractometer. The 2θ

dx.doi.org/10.1021/la302310y | *Langmuir* 2012, 28, 12044−12053

values were taken from 20° to 80° using Cu Kα radiation (λ value is 1.5416 Å). The average particle size is obtained from the most intense peak (311) by using the Debye−Scherrer formula. $d = 0.9\lambda/\beta \cos\theta$, where d is the particle size, β is the full width at half-maxima, λ is the incident copper Kα wavelength of 1.546 Å, and θ is the maximum peak position. The obtained patterns were verified by comparing it with the JCPDS data. The size distribution of nanoparticles was determined by dynamic light scattering using a Zetasizer-Nano (Malvern Instruments).

The small-angle X-ray scattering (SAXS) studies are carried out using Rigaku Ultima IV instrument. It uses Cu Kα (λ = 1.5418 Å) as X-ray source. The scattering intensity $I(q)$ was measured as a function of scattering vector ($q = (4\pi \sin\theta)/\lambda$). The scattering intensity plot is fitted with spherical model equation, $I(q) = |\Delta\rho|^2|(4\pi/q^3)[(\sin(qD/2) - (qD/2)\cos(qD/2)]|^2$, where D is the diameter of the particle and $\Delta\rho$ is the difference in electron density of particle and the dispersion medium. The most probable particle size is obtained from the distance distribution function.

3. RESULTS AND DISCUSSION

3.1. Properties of Nanoparticle and Pluronics. The XRD pattern of uncoated Fe_3O_4 nanoparticles at room temperature is shown in Figure 1a. The (220), (311), (400), (422), (511), and (440) diffraction peaks are indexed to cubic spinel structure. The average crystal size obtained from the Debye−Scherrer equation is found to be about 10 nm. The inverse spinel structure consists of oxide ions in the cubic close-packed arrangement in which 1/3 of tetrahedral interstices and 2/3 of octahedral interstices coordinate with oxygen where Fe(II) ions occupy the octahedral interstices, and half of the Fe(III) occupy the tetrahedral interstices with the remaining half of Fe(III) in octahedral interstices. For Fe_3O_4 phase, the parallel alignment of Fe(II) ions with Fe(III) ions in adjacent octahedral sites leads to a net magnetization. The measured value of the lattice constant, 0.838 nm, indicates that the sample is magnetite. Room temperature Mossbauer spectrum of Fe_3O_4 nanoparticle shows an intensified central doublet due to the superparamagnetic nature of particles and two sextets due to the two structurally different iron sites in the material.[76] The Mossbauer spectrum qualitatively establishes the presence of Fe^{2+} and Fe^{3+} ions in octahedral sites of magnetite crystal.

Figure 1b shows the size distribution profile of 25 wt % F108 with 5% Fe_3O_4, obtained from SAXS (red circle), and the size distribution of primary particle obtained from DLS (blue). The average particle size of nanoparticle obtained from DLS is ∼10 nm. The average cluster size obtained from SAXS is ∼46 nm. It should be noted that the DLS measurement is done on nanoparticles dispersion in water without triblock polymer where nanoparticles are stabilized by TMAOH surfactant. Therefore, DLS data show the hydrodynamic diameter of the nanoparticles, which is comparable to the average crystallite size obtained from XRD. The size distribution obtained from SAXS indicate larger aggregates formed in the polymeric matrix due to entanglement of particles due to the adsorbed polymeric coils. Figure 1c shows the schematic of TMAOH-coated Fe_3O_4 where the nanoparticle surface has a diffuse layer of negative hydroxide ion.

FT-IR analysis shows evidence for nanoparticle aggregation in presence of the Pluronic F108 copolymer (Figure 2). The FT-IR spectrum of nanocomposite shows that the C−O−C stretching band of pluronics broadens (at 1095 cm^{-1}) and shifts to 1114 cm^{-1}. The shift in the C−O−C stretching band is attributed to the formation of hydrogen bonds between oxygen of copolymers and water. Further, the broadening indicates that

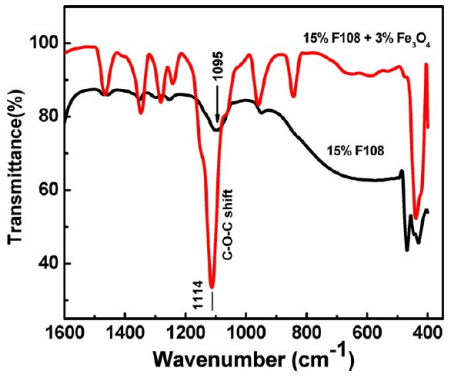

Figure 2. FT-IR spectrum of 15 wt % aqueous solution of Pluronic F108 in the absence and presence of 3 wt % Fe_3O_4 at 25 °C in the range of 1600−400 cm^{-1}.

the PEO−PPO−PEO block copolymer in aqueous solution have higher mobility.[77] Yang et al. have shown that transition metal ions can form crown-ether-type complexes with alkylene oxide segments in pluronic triblock copolymer.[78] Qu et al. have synthesized hollow nanospheres by using Pluronic F127 as capping source where they have shown that the capped F127 molecules induce aggregation of magnetite nanoparticle and form spherolites.[79] The binding of Pluronic F127 in aqueous dispersions of single- and multiwalled carbon nanotubes, studied by pulsed-field gradient NMR spectroscopy, shows that a minor fraction of polymers is bound to the carbon nanotubes.[80] The possible binding of F108 molecules on nanoparticles and the agglomeration of surfactant capped magnetic nanoparticles are shown in the schematic of Figure 1d.

3.2. Rheological Properties of Nanoparticles in a Weak Template of Triblock Copolymer. The dynamic moduli (elastic modulus G' and viscous modulus G'') as a function of temperature for 15 wt % F108 with five different concentrations (0, 1, 2, 3, and 5 wt %) of Fe_3O_4 nanoparticles is shown in Figure 3a. For 15 wt % of F108, the triblock copolymer micelles coexist with unimers.[81] For pure F108 copolymer solution, as the temperature increases, the G' starts increasing around 20 °C and reaches a maximum of 40 kPa around 40 °C. The increase in the elastic modulus with temperature is attributed to a transition from the solution of dissolved independent Gaussian unimers to a gel state through an intermediate micellar liquid. Figure 3b shows the gelation (T_g) temperature as a function of Fe_3O_4 concentration. The gelation temperature follows a power law scaling with concentration of nanoparticles.

At low temperature, the pure F108 remains as a micellar fluid where $G'' > G'$. With increasing temperature it is transformed to a soft gel ($G' > G''$) at moderate concentration (15 wt % F108) as a consequence of weak attraction between spherical micelles due to poor solvent condition. The transition from sol to soft gel occurs when aggregates of spherical micelles reach a percolation threshold, yielding sufficient structure to characteristic increase in elastic modulus.[82] For 1 wt % Fe_3O_4 loading, the nanocomposite shows a behavior similar to that of the pure copolymer. For 2 and 3 wt % Fe_3O_4 loading, the onset of increase in G' is shifted slightly to a lower temperature of ∼15 °C. Above 15 °C, the G' increases with temperature, followed by a plateau region in the temperature interval 25−45 °C, where the maximum value of G' is 30 kPa. Above 40 °C, the magnitude of G' decreases by a factor of 2, probably due to the

dx.doi.org/10.1021/la302310y | Langmuir 2012, 28, 12044−12053

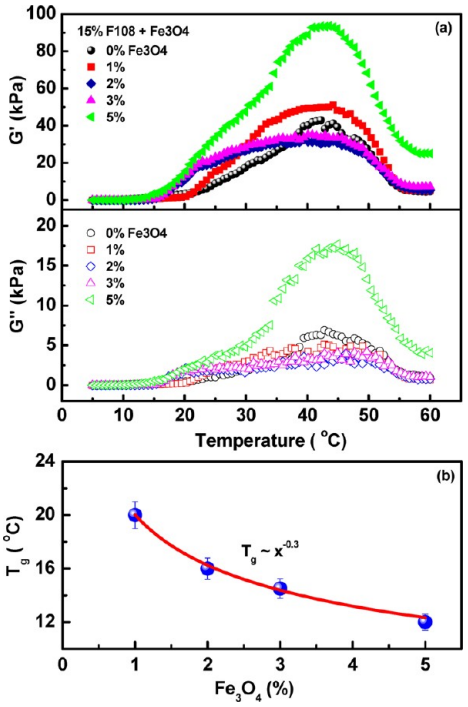

Figure 3. (a) Temperature-dependent elastic (G') and storage (G'') moduli for 15 wt % F108 at different Fe_3O_4 concentrations (0, 1, 2, 3, and 5%); applied strain is 0.5%. (b) Gelation (T_g) as a function of Fe_3O_4 concentration.

collapse of gel structure. In the presence of 5 wt % Fe_3O_4, no observable change in the onset of gelation is observed (~15 °C). However, the G' in the presence of 5 wt % nanoparticles reaches a maximum value of ~90 kPa, which is about 5 times the value of neat copolymer. Compared to pure F108, the onset of increase in the dynamic moduli of nanocomposite sample occurs at lower temperature. This observation is in sharp contrast with the temperature-dependent complex modulus variation observed in Pluronic F127 with silica nanoparticles of primary particle size of 7 nm where the increase in the moduli and the transition was much slower, which is attributed to the weakening of the crystallite state.[81] It should be noted that the size of the nanoparticles used in both the studies are smaller than the micelle size and the octahedral interstitial sites of the FCC crystal. Therefore, the observed difference may be attributed to the nature of conformation of nanoparticles within the polymeric template that alter the particle to micelle ratio. The ratio of the number of particles to micelles (N_P/N_M), particles to octahedral sites (N_P/N_O), and particles to tetrahedral sites (N_P/N_T) derived from the crystal unit cell dimension (d), particle radius (r), and particle volume fraction (Φ_P) by using simple geometrical ratio for an FCC crystal is given by[81] $N_P/N_M = \phi_P/[(1 - \phi_P)(16\pi/3)(r/d)^3]$, where $N_P/N_O = N_P/N_M$ and $N_P/N_T = 0.5(N_P/N_M)$. This equation assumes monodisperse particles and a uniform micelle crystal structure. These equations provide an approximate estimate of packing of composite. To find out the d-spacing of the cubic phase, SAXS experiment is performed on 25 wt % F108, which is found to be an ideal concentration for SAXS measurements. Figure 4 shows the SAXS profiles for 25 wt % F108 without and with 5 wt % of Fe_3O_4 nanoparticles at 25 °C. The intensity profile of pure F108 shows a higher order diffraction peak at a wave vector (q) ~ 0.038 $Å^{-1}$, confirming the presence of a

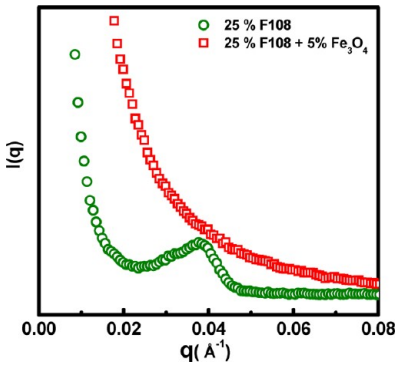

Figure 4. Variation of intensity as a function of scattering wave vector for 25 wt % F108 with and without Fe_3O_4 at 25 °C.

cubic structure of close-packed micelles. The intermicellar spacing (d) of the cubic crystal is found to be ~16.5 nm ($d = 2\pi/q$). Literature results show that the distance between adjacent micelle centers for pluronics F127 are 24.9 and 19.7 nm for 15 and 35 wt % polymers, respectively.[51] A recent study shows that the d-spacing of the micelles of the bcc gels of F127 in ethanol is in the range 12.1−14.3 nm.[83] For 1, 2, 3, and 5 wt % Fe_3O_4, the number of nanoparticles (N_P) in the solutions is 3.78 × 10^{21}, 7.62 × 10^{21}, 1.15 × 10^{22}, and 1.95 × 10^{22}, respectively. The calculation (where intermicellar spacing is used as 16.5 nm) shows that the ratio of the number of particles to micelles (N_P/N_M) for 1, 2, 3, and 5 wt % of Fe_3O_4 is 0.475, 0.96, 1.46, and 2.48, respectively. However, the ratio become much smaller than unity when the cluster size becomes larger. For example, for 22 nm size cluster, the (N_P/N_M) ratio for 1, 2, 3, and 5 wt % of Fe_3O_4 is 0.0056, 0.011, 0.017, and 0.029, respectively. In general, the templating quality is expected to be better when the ratio of particles to interstitial sites is of the order of one or less. When the ratio is above one, the crystalline order of the matrix can become distorted which will give rise to less correlation between the particles and the template structure. When the concentration of polymer in the matrix is large, the template should become stiffer crystals due to increased nanoparticle organization.

As the concentration of polymer is increased, the micelles are pushed closer, thereby reducing the dimensions of interstitial cavities, which eventually pushes the agglomerates out of the cavities. This results in a nanoparticle-rich and -poor phase within the templates. The first-order diffraction peak disappears when micelles are no longer close packed in a cubic structure. It is interesting to note that though the average crystallite size of nanoparticles is ~10 nm, the SAXS analysis shows that the average cluster size is about 46 nm with a spread across 10−300 nm, when the nanoparticles are within the supramolecular assembly formed by the triblock polymer. Interestingly, a previous study shows a similar polymer-mediated self-assembly of nanoparticles into structured ensembles.[84] Here, the assembly between 2 nm gold particles and polymer was achieved using the diaminotriazine−thymine three-point hydrogen-bonding interaction. When the cluster (particle) becomes larger than the intermicellar spacing, the effective incorporation of clusters inside the template structure become impossible, resulting in distortions in the close packing of F108 micelles where the gelation and mechanical properties shows different trends.[9]

Figure 5A shows the phase contrast optical microscopy images of 15 wt % F108 with 2 wt % Fe_3O_4. Figure 5B shows

dx.doi.org/10.1021/la302310y | Langmuir 2012, 28, 12044−12053

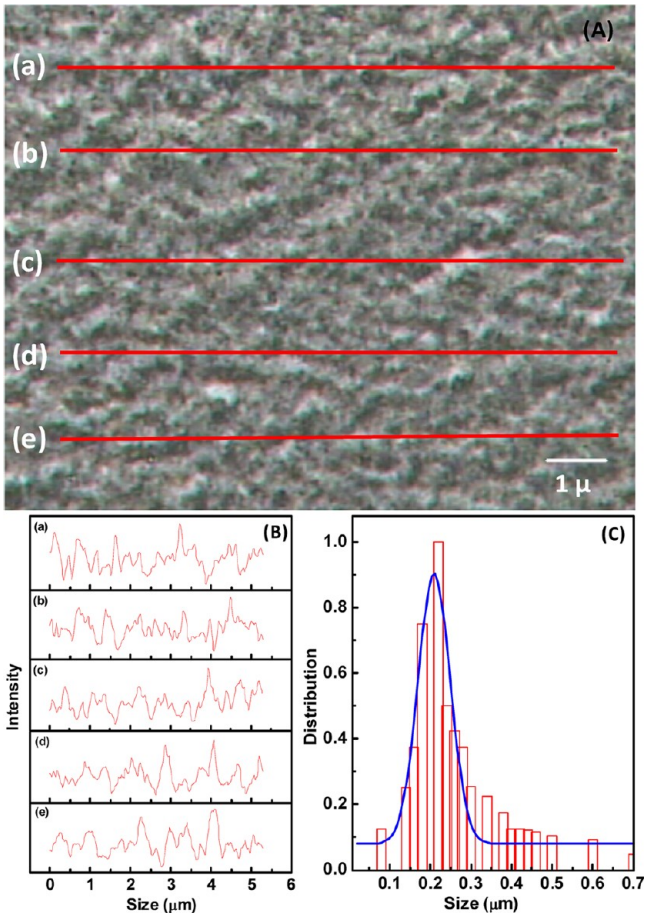

Figure 5. (A) Phase contrast optical microscopy images of 15 wt % F108 with 2 wt % Fe_3O_4. (B) Gray level line profiles across the lines a–e on the optical image is shown in (A). (C) Size distribution obtained from line profiles where the average size of the clusters within the triblock template is about 200 nm.

the line profiles across the optical image (lines a–e) shown in (A), and Figure 5C shows the size distribution obtained from several such line profiles. It was demonstrated that the soft gels near the hard gel boundary are defective versions of the cubic-packed gel, i.e., structured domains in an overall fluid matrix, and have higher elastic moduli than the more diffusive percolation structures.[83,85] At low temperature (15 °C), both pure copolymer and the nanoparticle–copolymer mixture are in the fluid state where a decrease in the gelation temperature with increase in nanoparticle concentration is observed. The dramatic reduction in the elastic modulus above 40 °C is probably due to the collapse of nanocomposite due to insufficient polymer concentrations to form a hard gel. Another plausible reason for the decrease in mechanical moduli at higher temperature is due to the deteriorating solvent conditions because of dehydration of EO chains and the eventual collapse of micellar polycrystals.[22]

Studies show that if the number of particles exceed the number of available template sites (structure rich in defects), the crystalline nature of the material is lost where the structure resembles a locally disordered amorphous fluid.[53,81] This results in the weakening of the nanocomposite properties. In concentrated samples, the formation of particle-poor and particle-rich phase occurs due to the stress caused by lattice incompatibility. At low particle loadings, the crystal structure is only slightly perturbed where particles are well templated. The slight reduction in the dynamic modulus observed at intermediate particle concentrations could be due to particle-rich and -poor regions within the matrix, which is evident in Figure 6. At intermediate nanoparticle loadings such phase

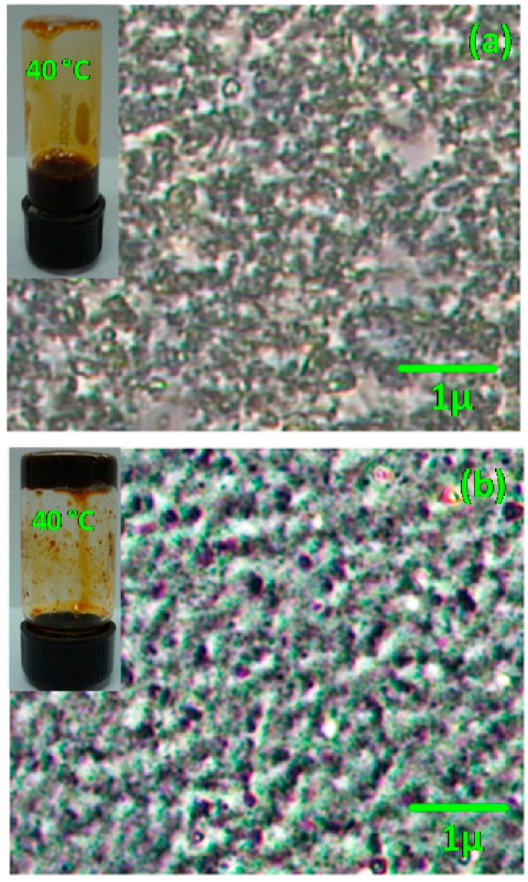

Figure 6. Optical microscopic images of 5 wt % nanoparticle in (a) 15 wt % and (b) 25 wt % of Pluronics F108 at 40 °C; inset shows the corresponding photographs of inverted sample vials. The sample with 25 wt.% F108 shows a gel-like behavior holding its weight on the inverted vial whereas the sample with 15 wt.% F108 exhibits a fluid-like behavior.

separation are indeed observed.[51] Figure 6 shows the optical microscopic images of 5 wt % nanoparticles in (a) 15 wt % and (b) 25 wt % of Pluronics F108 at 40 °C. The insets show the corresponding photographs of inverted sample vials. The sample with 25 wt.% F108 shows a gel-like behavior holding its weight on the inverted vial whereas the sample with 15 wt.% F108 exhibits a fluid-like behavior.

The changes in the macroscopic properties of nano-composite with nanoparticle loadings can be understood as follows: The addition of nanoparticles causes a change in the crystal structure, like swelling of the lattice or spontaneous phase separation driven by lattice incompatibility between the crystal containing particles and the pure micelle crystal. Such a phase separation results in thermodynamically favored states as the interfacial area between incompatible lattices is minimized. Finally, the excess particle will contribute to a loss of long-range order and the disruption of the crystal. The formed kinetically hindered, but locally disordered phase often resembles a glassy state.

dx.doi.org/10.1021/la302310y | *Langmuir* 2012, 28, 12044–12053

In F108 samples, prepared with different Fe_3O_4 loadings, amplitude sweep measurements are performed. The G' and G'' are measured while varying the strain amplitude between 0.1 and 100% at a fixed angular frequency of 1 rad/s. Amplitude sweep measurement is important to find the linear viscoelastic regime of samples and realize their response to strain deformation. The G' and G'' of 15 wt % F108 at different Fe_3O_4 concentrations (0, 3, and 5 wt %) at a temperature of 40 °C as a function of strain amplitude are shown in Figure 7. The

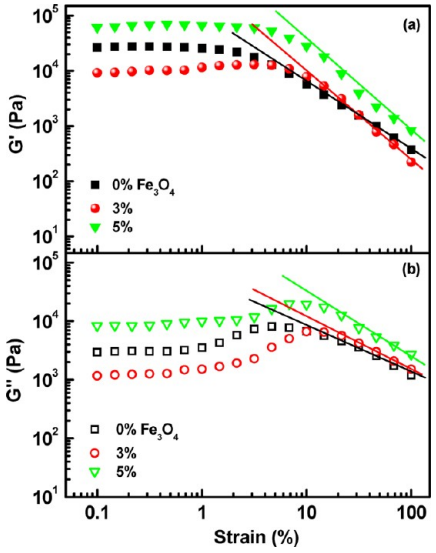

Figure 7. Amplitude sweep for 15 wt % F108 with two different Fe_3O_4 concentrations at temperature 40 °C: (a) G' and (b) and G''. Solid lines show power law fit.

samples show linear viscoelastic regime up to 5% strain, above which both G' and G'' are found to decrease with the strain amplitude that follow a power law scaling ($\gamma^{-\upsilon'}$). The exponents for 0, 3, and 5 wt % for G' are found to be 1.12, 1.48, and 1.52, respectively. The exponent of G'' for the same concentrations are found to be 0.75, 0.68, and 0.91, respectively. For samples with 3 wt % nanoparticles, the G'' decays slower compared to pure solutions (exponent value of ~0.69). However, for samples with 5 wt % of nanoparticles, the decay is faster than that of pure copolymer (exponent value of 0.91). The G' and G'' ratio for 3% nanoparticles is found to be ~2. But for pure copolymer and the one with 5% nanoparticle the ratio is found to be less than 1.5, which is the value for a typical Maxwellian fluid.[86] The exponents are found to be independent of copolymer concentration at larger oscillatory strain.[22] Amplitude sweep studies in pure F108 sample (0.25 g/cm^3) show that above a critical yield strain G' is found to decrease with strain γ_0 followed by a power law relation: $G'(\gamma_0) \sim \gamma_0^{-\upsilon'}$ and $G''(\gamma_0) \sim \gamma_0^{-\upsilon''}$.[22] The exponents are found to be $\upsilon' \sim 1.24 \pm 0.06$ and $\upsilon'' \sim 0.82 \pm 0.06$. The observed values of these exponents are comparable with the reported data.

Figure 8a–c shows the viscoelastic moduli as a function of frequency for 15 wt % of F108 at three different concentrations of Fe_3O_4 particles at 40 °C where the measurements are performed in the linear viscoelastic regime. In all the cases, the elastic modulus G' is found to be greater than the viscous modulus G'', indicating the elastic behavior. For pure copolymer, the G' decay weakly as a power law in the frequency range of 0.1–100 rad/s where the exponents for 0, 3, and 5 wt % Fe_3O_4 were 0.243, 0.102, and 0.356, respectively.

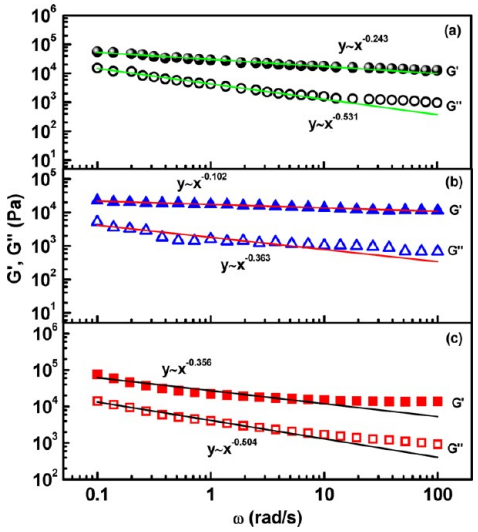

Figure 8. Viscoelastic moduli as a function of frequency for 15 wt % F108 with (a) 0 wt % Fe_3O_4, (b) 3 wt % Fe_3O_4, and (c) 5 wt % of Fe_3O_4 nanoparticles at 40 °C; applied strain is 0.5%.

The G'' also decays as a weak power law ($G''(\omega) \sim \omega^{-\delta''}$) where the exponents are found to be 0.63, 0.38, and 0.60 respectively for 0, 3, and 5 wt % of nanoparticle loading. The weak dependence of moduli on frequency indicates the occurrence of structural changes in the system. The observed decay of moduli suggests a weakening of the gel at larger frequencies. The larger exponent seen in the case of 5 wt % of particle loading suggests that the maximum weakening occur at this particle loading. Similar behavior is reported by Pozzo when 5 wt % silica nanoparticles are added in polymeric concentrations.[53] The weakening of nanocomposite gel at lower polymer concentrations can occur due to lowering of the chemical potential difference between the micelle corona and water matrix in the presence of added particles.[81] The weakening could also happen due to nanoparticle motion, which could be prominent at lower polymer concentration where particle motion can be large enough to affect the long-range crystal order because of the low modulus.[81]

Based on the rheology, microscopy, and SAXS results, the possible nanoparticle conformation within the templates of pluronics are shown in Figure 9. Figure 9a shows the cubic packing of F108 micelles, and Figure 9b shows the conformation of nanoparticles in the F108 micellar templates. The agglomeration of nanoparticle leads to a particle-poor and particle-rich regions above the gel temperature ($>T_g$). The approximate spacing between the nanoclusters are found to be about 200 nm, from microscopic image analysis, which was in good agreement with the SAXS results. This observation corroborates the fact that higher polymer concentration or reduced interstitial cavity dimensions can lead to nanoparticle-rich and -poor phases within the templates, which is schematically depicted in Figure 9.

3.3. Nanoparticles in Strong Templates of Triblock Polymers. The viscoelastic moduli as a function of temperature of a nanocomposite with 5 wt % Fe_3O_4 nanoparticles with two different concentrations of F108 (20 and 25 wt %) are shown in Figure 10. For pure F108 of 20 wt %, at 30 °C (the gelation temperature is 17 °C) the elastic modulus value is ~10 kPa, which increases by 7-fold when 5% nanoparticle is added. For 25 wt % F108, the G' value increases 8-fold (17 to 25 kPa

dx.doi.org/10.1021/la302310y | Langmuir 2012, 28, 12044–12053

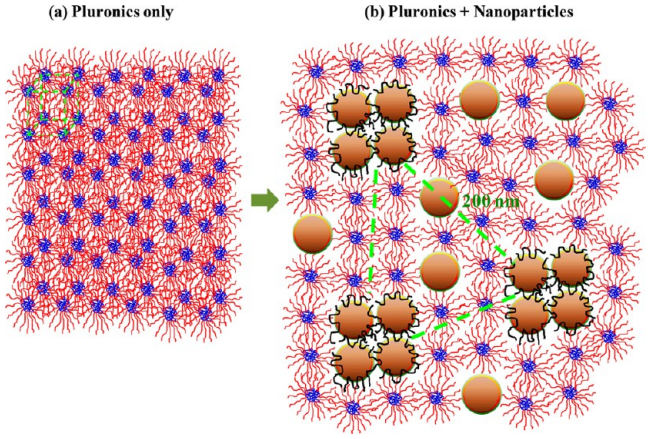

Figure 9. Schematic diagram showing the micellar packing of pure Pluronic F108 and with addition of nanoparticles: (a) cubic packing of F108 micelles and (b) the clustering of nanoparticle in F108 micellar templates leading to a particle-poor and particle-rich regions above gelation temperature ($>T_g$).

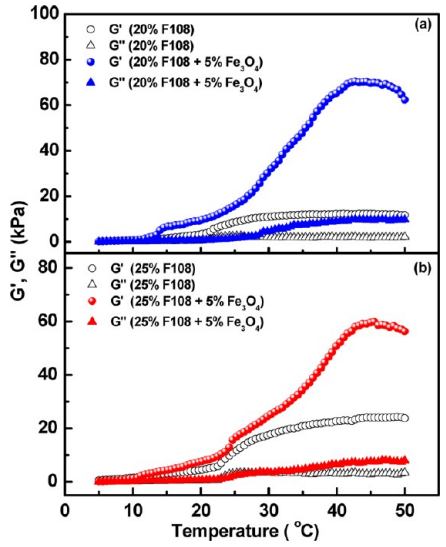

Figure 10. Viscoelastic moduli as a function of temperature for (a) 20 wt % F108 without and with 5 wt % Fe_3O_4 (b) 25 wt % F108 without and with 5 wt % Fe_3O_4. The measurements are performed at 0.5% strain and applied frequency of 1 rad/s.

at 30 °C) when 5 wt % of nanoparticles is added. Studies show that depending on the type of gels formed (cubic or hexagonal) the modulus can vary. A recent study shows that the storage modulus value in hexagonal gel is significantly lower than that of a cubic gel.[44] What is the reason for the observed lower storage modulus for 25 wt % copolymer composite compared to that of 20 wt %? An increase in the volume fraction of F108 micelles at higher polymer concentration (25 wt %) reduces the interstitial volume available for the nanoparticles, which in turn disturbs the formation of close packing of micelles. This can indeed reduce the storage modulus of the gel. Such a reduction in the storage modulus was observed by Krekhova et al. in ferrogels prepared by addition of magnetic nanoparticles in Pluronics P123 matrix.[44] Also, the increase in stiffness of the gel prevents particle motion when polymer concentrations was larger than 20 wt %.[81] Another study shows that the addition of 5 wt % silica nanoparticles (size ~7 nm) significantly reduces the modulus of 20 wt % F127 copolymer while nanocomposite with 30 wt % of F127 showed a higher modulus than the neat gel. The large increase in the modulus values of nanocomposite is attributed to the transfer of long-range order of the cubic crystal indirectly to nanoparticles by the excluded volume at higher temperature.[53] As the nanoparticles are solids, the polymer chains must stretch around these obstacles, causing a loss in conformational entropy that increases with particle radius.[87] The entropic penalty associated with chain stretching leads to transitions to different microstructures. In the absence of interactions, larger nanoparticles are expelled from bulk copolymers, whereas smaller particles remain in the interstitial spacing, which affects the spatial distribution of nanoparticles within the polymer matrix and its rheology. This seems to be the plausible reason for the observed dramatic changes in the rheology of nanocomposites.

3.4. Effect of Surfactant on Rheology of Nanocomposites. The viscoelastic modulus as a function of temperature for 15 wt % F108 with 2 wt % Fe_3O_4 at different SDS concentration is shown in Figure 11a. It is observed that the presence of 2 wt % Fe_3O_4 not only reduces the onset of gelation temperature but also improves the mechanical properties at lower temperatures. A collapse of modulus is observed above 42 °C in all the cases. Addition of 2 cmc (~16.2 mM) of SDS to the sample drastically reduces the elastic modulus value of nanocomposites. Further addition of SDS (5 and 10 cmc) shows a drastic reduction in the elastic behavior throughout the temperature range. This drastic

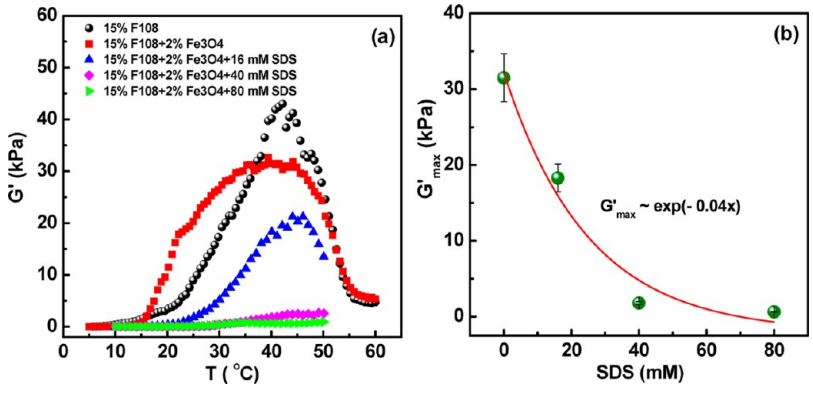

Figure 11. (a) Viscoelastic moduli as a function of temperature for nanocomposite samples in the presence of SDS of different concentrations. (b) G'_{max} as a function of SDS concentration at 40 °C.

dx.doi.org/10.1021/la302310y | *Langmuir* 2012, 28, 12044−12053

reduction in the mechanical properties of nanocomposite can be attributed to the destruction of templating structure due to the formation of pluronic−surfactant complexes. Figure 11b shows G'_{max} as a function of SDS concentration, where G'_{max} falls exponentially with the surfactant concentration with a weak decay length (∼0.04). To understand the effect of surfactant on nanocomposites, it is necessary to know the role of surfactant on triblock micellar assembly. The addition of anionic surfactants like SDS to triblock polymer results in the adsorption of DS^- chains to the hydrophobic central PPO core of the micelles, which imparts negative charges to mixed aggregates. The intra-aggregate repulsion leads to breakdown of large spherical micelles into smaller mixed micelles comprising of both triblock and SDS.[88,89] At low F108 concentrations, the surfactant micelles prevent self-assembly of F108 micelles due to effective electrostatic repulsion. However, at higher copolymer concentrations, the electrostatic repulsion among the surfactant headgroup reduces due to the penetration of hydrophilic PEO that favors micellar assembly and growth. Therefore, the addition of small amounts of SDS can result in the formation of large copolymer-rich charged complexes, while larger amount of SDS results in the breakup of these complexes and the formation of smaller surfactant-rich complexes.[90] The large decrease in the elastic modulus of the nanocomposite in the presence of SDS indicates a dramatic reduction in the mechanical properties. Further, the presence of charged species at higher cmc enhances the fluidity of the samples due to intermicellar repulsion that makes the condition unfavorable for the growth of micelles and a reduction in viscosity. This explains the reason for the observed variation in the elastic modulus with surfactant concentration. Studies on the influence of amphiphilic substances with Pluronic L64 shows that both rotational and translational mobility of the additive are significantly reduced by L64, and the additives significantly influence the conformation and association of the PPO block in L64.[31]

4. CONCLUSION

The thermogelling properties of F108−iron oxide nanocomposites are studied using rheometry and SAXS. Addition of 1−5 wt % of Fe_3O_4 nanoparticle in a weak polymeric template shows a decrease in the onset of gelation temperature and dramatic alteration in the viscoelastic moduli. The nanocomposite samples show a linear viscoelastic regime up to 5% strain, above which both G' and G'' follow a power law scaling ($\gamma^{-n'}$) with applied strain. The SAXS measurement in the strong gel shows an intermicellar spacing of 16.5 nm. The nanoparticle clusters size distribution obtained from SAXS is found to be in good agreement with the microscopic image analysis. The addition of an anionic surfactant to nanocomposites leads to a dramatic reduction in the viscoelastic properties due to the formation of smaller size surfactant-rich complexes. Our results show that the thermogelation is due to the clustering of nanoparticles rather than the close packing of F108 micelles.

AUTHOR INFORMATION

Corresponding Author

*E-mail philip@igcar.gov.in; Fax 00 91-44-27450356; Tel 00 91 44 27480232.

Notes

The authors declare no competing financial interest.

ACKNOWLEDGMENTS

J.P. thanks BRNS for funding for under perspective research grant on development of advance nanofluids. Authors thank Dr. T. Jayakumar, Director, Metallurgy and Materials Group, for fruitful discussions.

REFERENCES

(1) Alexandridis, P.; Hatton, T. A. *Colloids Surf., A* **1995**, *96*, 1.
(2) Chu, B. Structure and Dynamics of Block Copolymer Colloids. *Langmuir* **1995**, *11*, 414−421.
(3) Wu, C.; Liu, T.; Chu, B.; Schneider, D. K.; Graziano, V. Characterization of the PEO−PPO−PEO Triblock Copolymer and Its Application as a Separation Medium in Capillary Electrophoresis. *Macromolecules* **1997**, *30*, 4574−4583.
(4) Mortensen, K.; Almdal, K.; Schwahn, D.; Bates, F. S. Small-Angle Neutron Scattering Studies of the Phase Behavior and Mesophases of Homopolymers, Block Copolymers and Complex Mixtures. *J. Appl. Crystallogr.* **1997**, *30*, 702−707.
(5) Wanka, G.; Hoffmann, H.; Ulbricht, W. Phase Diagrams and Aggregation Behavior of Poly(oxyethylene)-Poly(oxypropylene)-Poly(oxyethylene) Triblock Copolymers in Aqueous Solutions. *Macromolecules* **1994**, *27*, 4145−4159.
(6) Prudhomme, R. K.; Wu, G. W.; Schneider, D. K. Structure and Rheology Studies of Poly(oxyethylene-oxypropylene-oxyethylene) Aqueous Solution. *Langmuir* **1996**, *12*, 4651−4659.
(7) Yardimci, H.; Chunga, B.; Harden, J. L.; Leheny, R. L. Phase Behavior and Local Dynamics of Concentrated Triblock Copolymer Micelles. *J. Chem. Phys.* **2005**, *123*, 244908.
(8) Mortensen, K.; Brown, W.; Norden, B. *Phys. Rev. Lett.* **1992**, *68*, 2340.
(9) Sun, K.; Raghavan, S. R. Thermogelling Aqueous Fluids Containing Low Concentrations of Pluronic F127 and Laponite Nanoparticles. *Langmuir* **2010**, *26*, 8015−8020.
(10) Nair, B. P.; Sharma, C. P. Poly(lactide-co-glycolide)−Laponite−F68 Nanocomposite Vesicles through a Single-Step Double-Emulsion Method for the Controlled Release of Doxorubicin. *Langmuir* **2012**, *28*, 4559−4564.
(11) McCormick, C. L.; Lowe, A. B. Recent Developments in Synthesis of Functional Water-Soluble Copolymers with Controlled Structures. *Acc. Chem. Res.* **2004**, *37*, 312−325.
(12) Eberle, A. P. R.; Wagner, N. J.; Castaneda-Priego, R. Dynamical Arrest Transition in Nanoparticle Dispersions with Short Range Interactions. *Phys. Rev. Lett.* **2011**, *106*, 105704.
(13) Madivala, B.; Vandebril, S.; Fransaer, J.; Vermant, J. Exploiting Particle Shape in Solid Stabilized Emulsions. *Soft Matter* **2009**, *5*, 1717−1727.
(14) Sabir, T. S.; Yan, D.; Milligan, J. R.; Aruni, A. W.; Nick, K. E.; Ramon, R. H.; Hughes, J. A.; Chen, Q.; Kurti, R. S.; Perry, C. C. Kinetics of Gold Nanoparticle Formation Facilitated by Triblock Copolymers. *J. Phys. Chem. C* **2012**, *116*, 4431−4441.
(15) Alexander, S.; Vos, W. M. d.; Castle, T. C.; Cosgrove, T.; Prescott, S. W. Growth and Shrinkage of Pluronic Micelles by Uptake and Release of Flurbiprofen: Variation of pH. *Langmuir* **2012**, *28*, 6539−6545.
(16) Slawecki, T. M.; Glinka, C. J.; Hammouda, B. Shear-Induced Micellar Crystal Structures in an Aqueous Triblock Copolymer Solution. *Phys. Rev. E* **1998**, *58*, R4084−R4087.
(17) Hamley, I. W. Structure and Flow Behaviour of Block Copolymers. *J. Phys.: Condens. Matter* **2001**, *13*, R643−R671.
(18) Pedersen, J. S.; Svaneborg, C. Scattering from Block Copolymer Micelles. *Curr. Opin. Colloid Interface Sci.* **2002**, *7*, 158−166.
(19) Habas, J. P.; Pavie, E.; Perreur, C.; Lapp, A.; Peyrelasse, J. Nanostructure in Block Copolymer Solutions: Rheology and Small-Angle Neutron Scattering. *Phys. Rev. E* **2004**, *70*, 061802.
(20) Jiang, J.; Burger, C.; Li, C.; Li, J.; Lin, M. Y.; Colby, R. H.; Rafailovich, M. H.; Sokolov, J. C. Shear-Induced Layered Structure of Polymeric Micelles by SANS. *Macromolecules* **2007**, *40*, 4016−4022.

(21) Trong, L. C. P.; Djabourov, M.; Ponton, A. Mechanisms of Micellization and Rheology of PEO−PPO−PEO Triblock Copolymers with Various Architectures. *J. Colloid Interface Sci.* **2008**, *328*, 278−287.
(22) Mohan, P. H.; Bandyopadhyay, R. Phase Behavior and Dynamics of a Micelle-Forming Triblock Copolymer System. *Phys. Rev. E* **2008**, *77*, 041803.
(23) Newby, G. E.; Hamley, I. W.; King, S. M.; Martin, C. M.; Terrill, N. J. Structure, Rheology and Shear Alignment of Pluronic Block Copolymer Mixtures. *J. Colloid Interface Sci.* **2009**, *329*, 54−61.
(24) Wanka, G.; Hoffmann, H.; Ulbricht, W. Phase Diagrams and Aggregation Behavior of Poly(oxyethylene)-Poly(oxypropylene)-Poly-(oxyethylene) Triblock Copolymers in Aqueous Solutions. *Macromolecules* **1994**, *27*, 4145−4159.
(25) Sun, M.; Wang, P.; Qiu, F.; Tang, P.; Zhang, H.; Yang, Y. Morphology and Phase Diagram of ABC Linear Triblock Copolymers: Parallel Real-Space Self-Consistent-Field-Theory Simulation. *Phys. Rev. E* **2008**, *77*, 016701.
(26) Guo, Z.; Zhang, G.; Qiu, F.; Zhang, H.; Yang, Y.; Shi, A. C. Discovering Ordered Phases of Block Copolymers: New Results from a Generic Fourier-Space Approach. *Phys. Rev. Lett.* **2008**, *101*, 028301.
(27) Bras, R. E.; Shull, K. R. Self-Consistent Field Theory of Gelation in Triblock Copolymer Solutions. *Macromolecules* **2009**, *42*, 8513−8520.
(28) Ulrich, K.; Galvosas, P.; Karger, J.; Grinberg, F. Effects of Self-Assembly on Diffusion Mechanisms of Triblock Copolymers in Aqueous Solution. *Phys. Rev. Lett.* **2009**, *102*, 037801.
(29) Fernandez, V. V. A.; Tepale, N.; Alvarez, J. G.; Lopez, J. H. P.; Macıas, E. R.; Bautista, F.; Pignon, F.; Rharbi, Y.; Corrales, R. G.; Manero, O.; Puig, J. E.; Soltero, J. F. A. Rheology of the Pluronic P103/Water System in a Semidilute Regime: Evidence of Non-equilibrium Critical Behavior. *J. Colloid Interface Sci.* **2009**, *336*, 842−849.
(30) Naskar, B.; Ghosh, S.; Moulik, S. P. Solution Behavior of Normal and Reverse Triblock Copolymers (Pluronic L44 and 10R5) Individually and in Binary Mixture. *Langmuir* **2012**, *28*, 7134−7146.
(31) Kriz, J. Interaction of Premicellar States of a PEO-PPO-PEO Triblock Copolymer with Partially Hydrophobic Substances: NMR Study. *J. Phys. Chem. B* **2012**, *116*, 4386−4393.
(32) Kasimova, A. O.; Pavan, G. M.; Danani, A.; Mondon, K.; Cristiani, A.; Scapozza, L.; Gurny, R.; Moller, M. Validation of a Novel Molecular Dynamics Simulation Approach for Lipophilic Drug Incorporation into Polymer Micelles. *J. Phys. Chem. B* **2012**, *116*, 4338−4345.
(33) Weiss, J.; Laschewsky, A. Temperature-Induced Self-Assembly of Triple-Responsive Triblock Copolymers in Aqueous Solutions. *Langmuir* **2011**, *27*, 4465−4473.
(34) Torija, M. A.; Choi, S.-H.; Lodge, T. P.; Bates, F. S. Large Amplitude Oscillatory Shear of Block Copolymer Spheres on a Body-Centered Cubic Lattice: Are Micelles Like Metals? *J. Phys. Chem. B* **2011**, *115*, 5840−5848.
(35) Tanner, S. A.; Amin, S.; Kloxin, C. J.; Zanten, J. H. v. Microviscoelasticity of Soft Repulsive Sphere Dispersions: Tracer Particle Microrheology of Triblock Copolymer Micellar Liquids and Soft Crystals. *J. Chem. Phys.* **2011**, *134*, 174903.
(36) O'Lenick, T. G.; Jin, N.; Woodcock, J. W.; Zhao, B. Rheological Properties of Aqueous Micellar Gels of a Thermo- and pH-Sensitive ABA Triblock Copolymer. *J. Phys. Chem. B* **2011**, *115*, 2870−2881.
(37) Maleki, A.; Kjoniksen, A.-L.; Zhu, K.; Nystrm, B. Temperature-Induced Aggregation Kinetics in Aqueous Solutions of a Temperature-Sensitive Amphiphilic Block Copolymer. *J. Phys. Chem. B* **2011**, *115*, 8975−8980.
(38) Lin, Y.; Daga, V. K.; Anderson, E. R.; Gido, S. P.; Watkins, J. J. Nanoparticle-Driven Assembly of Block Copolymers: A Simple Route to Ordered Hybrid Materials. *J. Am. Chem. Soc.* **2011**, *133*, 6513−6516.
(39) Kjoniksen, A.-L.; Zhu, K.; Behrens, M. A.; Pedersen, J. S.; Nystrm, B. Effects of Temperature and Salt Concentration on the Structural and Dynamical Features in Aqueous Solutions of Charged Triblock Copolymers. *J. Phys. Chem. B* **2011**, *115*, 2125−2139.
(40) Jiang, T.; Wang, L.; Lin, S.; Lin, J.; Li, Y. Structural Evolution of Multicompartment Micelles Self-Assembled from Linear ABC Triblock Copolymer in Selective Solvents. *Langmuir* **2011**, *27*, 6440−6448.
(41) Huff, A.; Patton, K.; Odhner, H.; Jacobs, D. T.; Clover, B. C.; Greer, S. C. Micellization and Phase Separation for Triblock Copolymer 17R4 in H_2O and in D_2O. *Langmuir* **2011**, *27*, 1707−1712.
(42) Hickey, R. J.; Haynes, A. S.; Kikkawa, J. M.; Park, S.-J. Controlling the Self-Assembly Structure of Magnetic Nanoparticles and Amphiphilic Block-Copolymers: From Micelles to Vesicles. *J. Am. Chem. Soc.* **2011**, *133*, 1517−1525.
(43) Deyerle, B. A.; Zhang, Y. Effects of Hofmeister Anions on the Aggregation Behavior of PEO−PPO−PEO Triblock Copolymers. *Langmuir* **2011**, *27*, 9203−9210.
(44) Krekhova, M.; Lang, T.; Richter, R.; Schmalz, H. Thermoreversible Hydroferrogels with Tunable Mechanical Properties Utilizing Block Copolymer Mesophases As Template. *Langmuir* **2010**, *26*, 19181−19190.
(45) Boucenna, I.; Royon, L.; Colinart, P.; Boudeville, M. A. G.; Mourchid, A. Structure and Thermorheology of Concentrated Pluronic Copolymer Micelles in the Presence of Laponite Particles. *Langmuir* **2010**, *26*, 14430−14436.
(46) Mezzenga, R.; Ruokolainen, J. Nanoparticles in the Right Place. *Nat. Mater.* **2009**, *8*, 926−928.
(47) Boucenna, I.; Royon, L.; Colinart, P. Effect of Laponite Clay Particles on Thermal and Rheological Properties of Pluronic Triblock Copolymer. *J. Therm. Anal. Calorim.* **2009**, *98*, 119−123.
(48) Paul, D. R.; Robeson, L. M. Polymer Nanotechnology: Nanocomposites. *Polymer* **2008**, *49*, 3187−3204.
(49) Rittigstein, P.; Priestley, R. D.; Broadbelt, L. J.; Torkelson, J. M. Model Polymer Nanocomposites Provide an Understanding of Confinement Effects in Real Nanocomposites. *Nat. Mater.* **2007**, *6*, 278−282.
(50) Pozzo, D. C.; Walker, L. M. Shear Orientation of Nanoparticle Arrays Templated in a Thermoreversible Block Copolymer Micellar Crystal. *Macromolecules* **2007**, *40*, 5801−5811.
(51) Pozzo, D. C.; Walker, L. M. Small-Angle Neutron Scattering of Silica Nanoparticles Templated in PEO−PPO−PEO Cubic Crystals. *Colloids Surf., A* **2007**, *294*, 117−129.
(52) Balazs, A. C.; Emrick, T.; Russell, T. P. Nanoparticle Polymer Composites: Where Two Small Worlds Meet. *Science* **2006**, *314*, 1107−1110.
(53) Pozzo, D. C.; Walker, L. M. Three-Dimensional Nanoparticle Arrays Templated by Self-Assembled Block-Copolymer Gels. *Macromol. Symp.* **2005**, *227*, 203−210.
(54) Lin, Y.; Boker, A.; He, J.; Sill, K.; Xiang, H.; Abetz, C.; Li, X.; Wang, J.; Emrick, T.; Long, S.; Wang, Q.; Balazs, A.; Russell, T. P. Self-Directed Self-Assembly of Nanoparticle/Copolymer Mixtures. *Nature* **2005**, *434*, 55−59.
(55) Chiu, J. J.; Kim, B. J.; Kramer, E. J.; Pine, D. J. Control of Nanoparticle Location in Block Copolymers. *J. Am. Chem. Soc.* **2005**, *127*, 5036−5037.
(56) Castelletto, V.; Ansari, I. A.; Hamley, I. W. Influence of Added Clay Particles on the Structure and Rheology of a Hexagonal Phase Formed by an Amphiphilic Block Copolymer in Aqueous Solution. *Macromolecules* **2003**, *36*, 1694−1700.
(57) Lin, Y.; Alexandridis, P. Temperature-Dependent Adsorption of Pluronic F127 Block Copolymers onto Carbon Black Particles Dispersed in Aqueous Media. *J. Phys. Chem. B* **2002**, *106*, 10834−10844.
(58) Sidorov, S. N.; Bronstein, L. M.; Valetsky, P. M.; Hartmann, J.; Colfen, H.; Schnablegger, H.; Antonietti, M. Stabilization of Metal Nanoparticles in Aqueous Medium by Polyethyleneoxide−Polyethyleneimine Block Copolymers. *J. Colloid Interface Sci.* **1999**, *212*, 197−211.

(59) Moller, M.; Spatz, J. P. Mineralization of Nanoparticles in Block Copolymer Micelles. *Curr. Opin. Colloid Interface Sci.* **1997**, *2*, 177−187.
(60) Tamborini, E.; Ghofraniha, N.; Oberdisse, J.; Cipelletti, L.; Ramos, L. Structure of Nanoparticles Embedded in Micellar Polycrystals. *Langmuir* **2012**, *28*, 8562−8570.
(61) Alexandridis, P.; Tsianou, M. Block Copolymer-Directed Metal Nanoparticle Morphogenesis and Organization. *Eur. Polym. J.* **2011**, *47*, 569−583.
(62) Starra, F. W.; Douglas, J. F.; Glotzer, S. C. Origin of Particle Clustering in a Simulated Polymer Nanocomposite and Its Impact on Rheology. *J. Chem. Phys.* **2003**, *119*, 1777−1788.
(63) Galicia, J. A.; Sandre, O.; Cousin, F.; Guemghar, D.; Menager, C.; Cabuil, V. Designing Magnetic Composite Materials Using Aqueous Magnetic Fluids. *J. Phys.: Condens. Matter* **2003**, *15*, S1379−S1402.
(64) Biswas, S.; Belfield, K. D.; Das, R. K.; Ghosh, S.; Hebard, A. F. Block Copolymer-Mediated Formation of Superparamagnetic Nanocomposites. *Chem. Mater.* **2009**, *21*, 5644−5653.
(65) Yang, T. I.; Brown, R. N. C.; Kempel, L. C.; Kofinas, P. Magneto-Dielectric Properties of Polymer-Fe_3O_4 Nanocomposites. *J. Magn. Magn. Mater.* **2008**, *320*, 2714−2720.
(66) Reinicke, S.; Dohler, S.; Tea, S.; Krekhova, M.; Messing, R.; Schmidt, A. M.; Schmalz, H. Magneto-responsive Hydrogels Based on Maghemite/Triblock Terpolymer Hybrid Micelles. *Soft Matter* **2010**, *6*, 2760−2773.
(67) Qin, J.; Asempah, I.; Laurent, S.; Fornara, A.; Muller, R. N.; Muhammed, M. Injectable Superparamagnetic Ferrogels for Controlled Release of Hydrophobic Drugs. *Adv. Mater.* **2009**, *21*, 1354−1357.
(68) Messing, R.; Schmidt, A. M. Perspectives for the Mechanical Manipulation of Hybrid Hydrogels. *Polym. Chem.* **2011**, *2*, 18.
(69) Satarkar, N. S.; Biswal, D.; Hilt, J. Z. Hydrogel Nanocomposites: a Review of Applications As Remote Controlled Biomaterials. *Soft Matter* **2010**, *6*, 2364−2371.
(70) Schexnailder, P.; Schmidt, G. Nanocomposite Polymer Hydrogels. *Colloid Polym. Sci.* **2009**, *287*, 1−11.
(71) Monz, S.; Tschope, A.; Birringer, R. Magnetic Properties of Isotropic and Anisotropic $CoFe_2O_4$-Based Ferrogels and Their Application As Torsional and Rotational Actuators. *Phys. Rev. E* **2008**, *78*, 021404.
(72) Ghosh, S.; Yang, C.; Cai, T.; Hu, Z.; Neogi, A. Oscillating Magnetic Field-Actuated Microvalves for Micro- and Nanofluidics. *J. Phys. D: Appl. Phys.* **2009**, *42*, 135501.
(73) Satarkar, N. S.; Hilt, J. Z. Magnetic Hydrogel Nanocomposites for Remote Controlled Pulsatile Drug Release. *J. Controlled Release* **2008**, *130*, 246−251.
(74) Anderson, K. W.; Hilt, J. Z. Hydrogel Nanocomposites: Biomedical Applications, Biocompatibility, and Toxicity Analysis. In *Safety of Nanoparticles*; Springer: New York, 2009.
(75) Shima, P. D.; Philip, J.; Raj, B. Synthesis of Aqueous and Nonaqueous Iron Oxide Nanofluids and Study of Temperature Dependence on Thermal Conductivity and Viscosity. *J. Phys. Chem. C* **2010**, *114*, 18825−18833.
(76) Gnanaprakash, G.; Philip, J.; Jayakumar, T.; Raj, B. Effect of Digestion Time and Alkali Addition Rate on Physical Properties of Magnetite Nanoparticles. *J. Phys. Chem. B* **2007**, *111*, 7978.
(77) Su, Y.-l.; Liu, H.-z.; Wang, J.; Chen, J.-y. Study of Salt Effects on the Micellization of PEO-PPO-PEO Block Copolymer in Aqueous Solution by FTIR Spectroscopy. *Langmuir* **2002**, *18*, 865−871.
(78) Yang, P.; Zhao, D.; Margolese, D. I.; Chmelka, B. F.; Stucky, G. D. Generalized Syntheses of Large-Pore Mesoporous Metal Oxides with Semicrystalline Frameworks. *Nature* **1998**, *396*, 152−155.
(79) Qu, X.-F.; Yao, Q.-Z.; Zhou, G.-T.; Fu, S.-Q.; Huang, J.-L. Formation of Hollow Magnetite Microspheres and Their Evolution into Durian-like Architectures. *J. Phys. Chem. C* **2010**, *114*, 8734−8740.
(80) Frise, A. E.; Pages, G.; Shtein, M.; Bar, I. P.; Regev, O.; Furo, I. Polymer Binding to Carbon Nanotubes in Aqueous Dispersions: Residence Time on the Nanotube Surface As Obtained by NMR Diffusometry. *J. Phys. Chem. B* **2012**, *116*, 2635−2642.
(81) Pozzo, D. C.; Hollabaugh, K. R.; Walker, L. M. Rheology and Phase Behavior of Copolymer-Templated Nanocomposite Materials. *J. Rheol.* **2005**, *49*, 759−782.
(82) Li, H.; Yu, G.-E.; Price, C.; Booth, C.; Fairclough, J. P. A.; Ryan, A. J.; Mortensen, K. Mesophase Behavior of Aqueous Micellar Solutions of Triblock Copolymers of Ethylene Oxide and 1,2-Butylene Oxide (Type $E_mB_nE_m$). *Langmuir* **2003**, *19*, 1075−1081.
(83) Chaibundit, C.; Ricardo, N. M. P. S.; Ricardo, N. M. P. S.; Muryn, C. A.; Madec, M. B.; Yeates, S. G.; Booth, C. Effect of Ethanol on the Gelation of Aqueous Solutions of Pluronic F127. *J. Colloid Interface Sci.* **2010**, *351*, 190−196.
(84) Boal, A. K.; Ilhan, F.; DeRouchey, J. E.; Albrecht, T. T.; Russell, T. P.; Rotello, V. M. Self-Assembly of Nanoparticles into Structured Spherical and Network Aggregates. *Nature* **2000**, *13*, 746−748.
(85) Prud'homme, R. K.; Wu, G.; Schneider, D. K. Structure and Rheology Studies of Poly(oxyethylene−oxypropylene−oxyethylene) Aqueous Solution. *Langmuir* **1996**, *12*, 4651−4659.
(86) Miyazaki, K.; Wyss, H. M.; Weitz, D. A.; Reichman, D. R. Nonlinear Viscoelasticity of Metastable Complex Fluids. *Europhys. Lett.* **2006**, *75*, 915−921.
(87) Thompson, R. B.; Ginzburg, V. V.; Matsen, M. W.; Balazs, A. C. Predicting the Mesophases of Copolymer-Nanoparticle Composites. *Science* **2001**, *292*, 2469−2472.
(88) Hecht, E.; Hoffmann, H. Interaction of ABA Block Copolymers with Ionic Surfactants in Aqueous Solution. *Langmuir* **1994**, *10*, 86−91.
(89) Sastry, N. V.; Hoffmann, H. Interaction of Amphiphilic Block Copolymer Micelles with Surfactants. *Colloids Surf. A* **2004**, *250*, 247−261.
(90) Nambam, J. S.; Philip, J. Effects of Interaction of Ionic and Nonionic Surfactants on Self-Assembly of PEO−PPO−PEO Triblock Copolymer in Aqueous Solution. *J. Phys. Chem. B* **2012**, *116*, 1499−1507.